Dalton Transactions

ROYAL SOCIETY OF CHEMISTRY

PAPER

View Article Online
View Journal | View Issue

Cite this: *Dalton Trans.*, 2025, **54**, 13257

Short but promising – how nature modulates the antimicrobial activity of proline-rich fragment of salivary MUC-7

Jakub Gawłowski,[a] Anna Ślusarczyk,[a] Klaudia Szarszoń,[a] Fabio Zobi,[b] Tomasz Janek[c] and Joanna Wątły*[a]

Antimicrobial peptides (AMPs), including mucin-derived sequences, play a vital role in host defense at mucosal surfaces by modulating microbial interactions and supporting innate immunity. However, their susceptibility to proteolytic cleavage limits their protective efficacy. This study investigates the peptide FPNPHQPPKHPDK (L1), derived from human salivary mucin MUC7, and its proteolytic fragments L2 (FPNPHQPPK) and L3 (HPDK), generated by trypsin cleavage. Using a combination of potentiometry, UV–vis spectroscopy, circular dichroism (CD), electron paramagnetic resonance (EPR), electrospray ionization mass spectrometry (ESI-MS), density functional theory (DFT) calculations, and antimicrobial assays, we elucidate the structural and thermodynamic aspects of metal ion coordination with Cu(II) and Zn(II), and assess their impact on antimicrobial efficacy. Our findings reveal that the L3 fragment forms the most thermodynamically stable complexes with both Cu(II) and Zn(II) ions, and exhibits the strongest antimicrobial activity, which is pH-dependent. These results suggest a mechanism involving metal sequestration, consistent with the concept of 'nutritional immunity'. Notably, natural proteolytic processing of the parent peptide enhances its functional properties upon metal coordination. This highlights a potential evolutionary advantage of peptide fragmentation in modulating antimicrobial activity, supporting the development of MUC7-derived peptides as promising templates for metal-based antimicrobial agents.

Received 16th June 2025,
Accepted 10th August 2025

DOI: 10.1039/d5dt01418b

rsc.li/dalton

Introduction

Saliva, as a rich reservoir of antimicrobial molecules, especially AMPs, is the first line of defense against pathogenic microbes.[1] The pH of saliva plays a crucial role as a diagnostic and prognostic biomarker in oral health, but also has a huge impact on the activity of antimicrobial molecules present in the oral cavity. Normal unstimulated saliva in healthy individuals exhibits a pH range of approximately 6.2–7.6, with an average around 6.7, and rarely drops below 6.3 under resting conditions.[2,3] Such near-neutral pH is maintained by salivary buffering systems and is essential for protecting dental hard tissues.[4,5] In pathological states, salivary pH shows distinct shifts: it becomes more alkaline in conditions like generalized chronic gingivitis,[2] yet tends toward acidity in more severe diseases such as generalized chronic periodontitis. Following food intake-particularly meals rich in fermentable carbohydrates such as sucrose, glucose, or starch-salivary pH can rapidly drop below 5.5 due to acid production by cariogenic bacteria like *Streptococcus mutans*.[6,7]

Salivary AMPs include, *e.g.* histatins, defensins, chemokines, cathelicidins, and mucins.[8–10] Mucins are a family of glycoproteins that are present not only in saliva, where they are responsible for its viscosity, but also are present in different types of mucus, *e.g.* in the bile, stomach, and intestines, where they protect mucous membranes against the action of digestive enzymes.[11,12] Although mucins can differ significantly in molecular mass, they all contain characteristic tandem-repeating domains – rich in amino acid residues such as serine, proline, and threonine.[13,14] These domains are sites of extensive glycosylation of the peptide chain (oligosaccharide chains can constitute up to 90% of the molecular mass of the resulting glycoprotein).[15] Because of these post-translational modifications, mucins can perform specific functions. In humans, the presence of 16 mucins has been identified.[13] They are divided into transmembrane and secretory mucins. MUC5B and MUC7 are two secretory mucins present in saliva.[16]

The MUC7 (Fig. 1) is a low molecular mass protein secreted into saliva by the submandibular and sublingual glands.[17] The

[a]*Faculty of Chemistry, University of Wrocław, F. Joliot-Curie 14, 50-383 Wrocław, Poland. E-mail: joanna.watly2@uwr.edu.pl*
[b]*Department of Chemistry, Fribourg University, Chemin Du Musée 9, 1700 Fribourg, Switzerland*
[c]*Department of Biotechnology and Food Microbiology, Wrocław University of Environmental and Life Sciences, Chełmońskiego 37, 51-630 Wrocław, Poland*

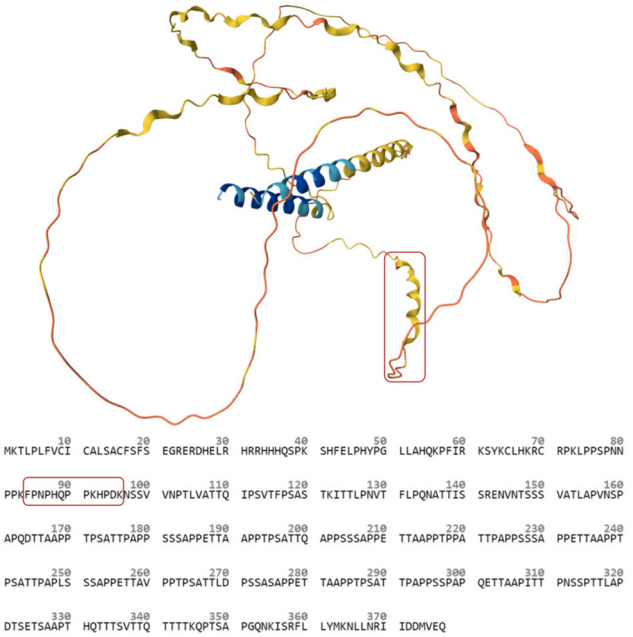

Fig. 1 The AlphaFold predicted structure and amino acid sequence of MUC7 (UniProtKB: Q8TAX7). The analysed region of this biomolecule (FPNPHQPPKHPDK) is highlighted in orange.

amino acid sequence of MUC7 can be divided into 6 regions: (1) signal peptide (aa^{1-20}); (2) Domain 1 (D1) (aa^{21-71}); (3) D2 (aa^{72-164}); (4) D3 ($aa^{165-303}$); (5) D4 ($aa^{304-355}$) and (6) D5 ($aa^{356-377}$).[18] The central region (D3 and D4) consists of a sequence of 23 amino acids that is repeated six times: TTAAPPTPSATTPAPPSSSAPPE (PTS domain). The main role of this protein is to maintain proper bacterial flora in the oral cavity.[19–21]

The D1 domain at the N-terminal region has a similar sequence to the well-known AMP, histatin 5 (Hst-5), and shows antibacterial and antifungal activity.[22]

In this study, we focus on the Pro-rich, FPNPHQPPKHPDK (L1) peptide, which is a proteolytic product of the MUC7 glycoprotein,[23] and on two fragments derived from this sequence, which can be naturally cleaved by trypsin at the most susceptible site, between the amino acids Lys and His, resulting in two shorter peptides: FPNPHQPPK (L2) and HPDK (L3) (Fig. 2, Fig. S1).

Antimicrobial peptides often contain repeating patterns of specific amino acids. Among the most common are peptides rich in tryptophan (Trp), arginine (Arg), histidine (His), cysteine (Cys), and proline (Pro) – as in the peptide under investigation.[24] AMPs primarily exert their activity through two major mechanisms: (i) membrane-targeting mechanisms, where peptides disrupt the structural integrity of microbial cell membranes, and (ii) non-membrane-targeting mechanisms, which involve the inhibition of intracellular processes such as nucleic acid, protein, and enzyme synthesis, ultimately leading to microbial growth arrest and inhibition of reproduction.[25]

Proline-rich antimicrobial peptides (PrAMPs) represent a distinct class of AMPs with primarily intracellular activity, typically inhibiting bacterial protein synthesis. For example, bactenecin 7 (Bac7) and the dolphin-derived peptide Tur1A exert their inhibitory effects by interacting with ribosomes, blocking translation by preventing the transition from the initiation to the elongation phase.[26,27] Similarly, the Api137 peptide inhibits translation by arresting the release factor on the ribosome.[28] Interestingly, proline-rich proteins (PRPs) constitute a significant fraction (nearly 70%) of the total salivary proteins[29] and play a crucial role in interspecies bacterial interactions, thereby contributing to the maintenance of a balanced oral microbiome.[30]

Proline is a structurally unique amino acid, essential for defining protein structure and function. Specifically, (i) proline facilitates the formation of secondary structural elements such as the polyproline II helix and (ii) induces β-turn formation, leading to a 'bent' peptide conformation.[30–33] Some studies suggest that proline-rich antimicrobial peptides could serve as a promising foundation for the development of novel therapeutics against antibiotic-resistant bacteria and may also enhance drug delivery efficiency.[34–36]

Literature data strongly suggest that the presence of metal ions often enhances – or, in some cases, triggers the antimicrobial activity of AMPs, influencing factors such as net charge, secondary structure, or participation in processes like 'nutritional immunity' or the generation of free radicals.[37–43]

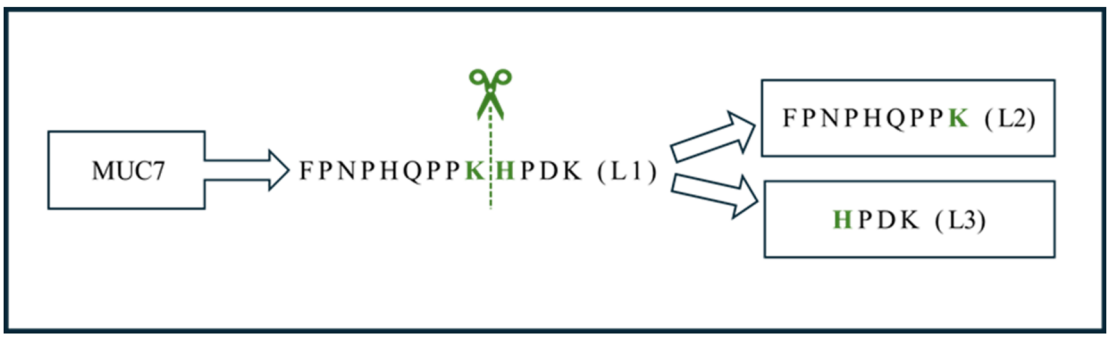

Fig. 2 The selected peptide fragment (in the middle), which underwent cleavage by proteolytic enzymes, was divided into two distinct peptides. The amino acids at which enzymatic cleavage by trypsin occurred are highlighted in green.

Given that saliva contains substantial concentrations of metal ions, including zinc(II) and copper(II),[44] and that the L1, L2, and L3 peptides derived from the MUC7 glycoprotein possess amino acid residues capable of effectively binding these ions (*e.g.* the imidazole ring of histidine or the amino-terminal group), it is imperative to explore the influence of these metal ions on (i) coordination modes, (ii) secondary structure, and (iii) the antimicrobial properties of these salivary peptides.

Therefore, this study aims to investigate the impact of proteolytic hydrolysis on the biological activity of peptides derived from MUC7 and their complexes with metal ions, specifically assessing whether they retain the antimicrobial and metal-coordinating properties of the parent peptide. Furthermore, we seek to elucidate how metal ion coordination influences the stability and efficacy of these peptides, which could provide valuable insights for optimizing their potential therapeutic applications.

Experimental section

Materials

The fragments of the salivary glycoprotein MUC7 – FPNPHQPPKHPDK (L1), FPNPHQPPK (L2), and HPDK (L3) were commercially synthesized by KareBay™ Biochem company with a certified purity of 98% (Fig. S2). All peptides were free at both the C- and N-termini. Analytical-grade reagents were used in all experiments. The concentrations of Cu(II) and Zn(II) perchlorate hexahydrate (Sigma-Aldrich) solutions were determined using inductively coupled plasma optical emission spectrometry (ICP-OES). A 0.1 M NaOH solution (Supelco) was potentiometrically standardized with an acidic potassium phthalate solution (C = 0.004 M, Sigma-Aldrich). Double-distilled water was used to prepare all samples. The ionic strength (I = 0.1 M) was adjusted by dissolving $NaClO_4$ (Sigma-Aldrich). Peptides for potentiometric titrations were dissolved in 0.004 M $HClO_4$ (prepared from 70–72% perchloric acid, Supelco) with an ionic strength of 0.1 M $NaClO_4$. All samples were weighed using an analytical balance (Sartorius R200D).

Trypsin digestion experiment

A sample containing the peptide FPNPHQPPKHPDK (1 mg) was incubated with trypsin (5 mg mL^{-1}, 100 μL) in ammonium carbonate buffer (100 mM, pH 8.2, 900 μL) for 24 hours at 37 °C in a water bath. The reaction was stopped by the addition of trifluoroacetic acid (5% TFA) to lower the pH to approximately 3.5. The resulting mixture was transferred to Vivaspin 500 concentrators (PES membrane, 5000 Da), centrifuged, and analyzed using a JEOL JMS-S3000 SpiralTOF™-plus Ultra-High Mass Resolution MALDI-TOF MS with a cationic matrix (z = +1). A control sample containing only trypsin and buffer was prepared as a reference. The results were analyzed using the msTornado Analysis software (version 2.0.11.1). The matrix compound used to produce the matrix solution was sinapic acid. Sinapic acid (10 mg) was dissolved in 1 mL of 50/50 acetonitrile/water solvent containing 0.1% TFA. The sample and matrix mix were mixed 1 : 1 by volume and spotted onto a 96 well stainless steel plate and allowed to air dry. The results were analyzed using the msTornado Analysis software (version 2.0.11.1).

Potentiometric measurements

The stability constants for all ligands and their complexes with metal ions Cu(II) and Zn(II) were calculated based on titration curves in the pH range 2.0–12.0. at 25 °C in a total volume of 2.6 mL. Potentiometric measurements were carried out for all samples, in 0.004 M $HClO_4$ solution with an ionic strength I = 0.1 M $NaClO_4$. The apparatus comprised a Metrohm Titrando 905 titrator equipped with a Mettler Toledo InLab Semi-Micro combined pH electrode. The glass cell, maintained at a constant temperature, was fitted with a magnetic stirring device, a microburet for precise liquid dispensing, and a tube system for argon flow. Solutions were titrated with 0.1 M carbonate-free NaOH. Before starting the experiment, electrodes were calibrated by titration of 0.004 M $HClO_4$ with 0.1 M NaOH using a total volume of 3 mL. Determination of concentration and purity level was possible through using the Gran method.[45] The ligand concentration was 0.0004 M, and the Cu(II) and Zn(II) to ligand ratio was 0.9 : 1. Calculations of constant stability were performed in HYPERQUAD 2006.[46] The standard deviations were computed by using HYPERQUAD 2006 and referenced to random errors only. The hydrolysis constants of Cu(II) and Zn(II) were taken from the literature and used in these calculations.[47] The speciation and competition diagrams were computed using the HYSS program and visualized in the Origin 2024 program.[48,49]

Mass spectrometric measurements

The experiment was performed using Bruker Compact QTOF (Bruker Daltonik, Bremen, Germany), equipped with an electrospray ionization source with an ion funnel. The spectra were recorded in positive ion modes, within a mass-to-charge ratio (m/z) range of 150–3000. The experimental conditions included dry nitrogen gas, T = 180 °C, a capillary voltage of 4500 V, and an ion energy of 5 eV. The solutions of ligands and their complexes with Cu(II) and Zn(II) ions ([L] = 0.0001 M, molar ratio M : L = 1 : 1) were prepared by dissolving in a 50 : 50 mixture of water and methanol. The instrument was calibrated externally with the Low Concentration Tuning Mix ESI-ToF (Agilent Technologies, Santa Clara, CA, USA). The samples were infused at a flow rate of 3 μL min^{-1}. The obtained spectra were analyzed using the Bruker Compass DataAnalysis 6.1 program.

Spectroscopic studies

The absorption spectra were recorded on a Jasco V-750 spectrophotometer, while circular dichroism (CD) spectra were obtained by using a Jasco J-1500 CD spectropolarimeter; in both cases, a quartz cuvette with an optical path length of 1 cm was used. In the far-UV CD experiment (wavelength range 180–250 nm), a quartz cuvette with an optical path length of 0.2 mm was used. All spectrophotometric measure-

ments were conducted in a pH range of 3.0–11.5 at 25 °C. The pH of the samples was adjusted by adding NaOH and $HClO_4$ solutions. Concentrations of samples were similar to those used in the potentiometric titration. The metal-to-ligand ratio was 0.9 : 1. Electron paramagnetic resonance (EPR) spectra were recorded on a Bruker ELEXSYS E500 CW-EPR spectrometer at a band frequency of 9.5 GHz. Ligands were dissolved in an aqueous solution of 0.004 M $HClO_4$ with ionic strength 0.1 M ($NaClO_4$). Ethylene glycol (25%) was used as a cryoprotectant due to the measurements were conducted at a liquid nitrogen temperature (77 K) within a pH range of 3–11. The concentration of Cu(II) was 0.001 M, and the metal : ligand ratio was 0.9 : 1. The EPR parameters were determined by simulating the spectra and comparing them with the experimental data in Bruker's WinEPR SimFonia (version 1.2) software. $A_{\|}$ spectra were analyzed and visualized using Origin 2024.[49]

In vitro antimicrobial activity of peptides and peptide–metal ion systems

Antimicrobial activity of peptides and their complexes was characterized against human pathogenic strains that may occur in the oral cavity. Four reference strains from the American Type Culture Collection (ATCC), namely *Escherichia coli* 25922, *Pseudomonas aeruginosa* 15442, *Enterococcus faecalis* 29212, *Staphylococcus aureus* 25923, two from the Polish Collection of Microorganisms (PCM), namely *Streptococcus mutans* 2502 and *Streptococcus sanguinis* 2335, and *Candida albicans* SC5314 were used for antimicrobial activity assay.[50] *E. coli* ATCC 25922, *P. aeruginosa* ATCC 15422, *E. faecalis* ATCC 29212, and *S. aureus* ATCC 25923 were grown at 37 °C in Mueller–Hinton broth (MHB) (Merck Millipore, Darmstadt, Germany). *S. mutans* PCM 2502 and S. *sanguinis* PCM 2335 were cultured in Brain Heart Infusion (BHI) broth (Merck Millipore, Darmstadt, Germany) and incubated overnight anaerobically (85% N_2, 10% H_2, and 5% CO_2) at 37 °C. *C. albicans* SC5314 was grown aerobically at 37 °C on Yeast Peptone Dextrose (YPD) broth (A&A Biotechnology, Gdańsk, Poland).

Bacterial susceptibility assay

To determine the minimal inhibitory concentrations (MIC) of the studied systems required to inhibit the growth of strains, the serial broth microdilution method was employed.[51] Briefly, two-fold serial dilutions of each peptide/complex in MHB, BHI, and YPD broth buffered with 0.01 M MES buffer, pH 5.4 (Merck Millipore, Darmstadt, Germany) or 0.01 M HEPES buffer, pH 7.4 (Merck Millipore, Darmstadt, Germany) at a volume of 100 μL were prepared in 96-well flat-bottomed microtiter plates (Sarstedt, Nümbrecht, Germany). The final concentration of each system ranged from 7.8 to 500 μg mL^{-1}. Control wells, including negative and growth controls, did not contain the tested compounds. In addition, antimicrobial assays were performed using Cu(II) and Zn(II) ion concentrations ranging from 0.5 to 65 μg mL^{-1}, corresponding to the metal content in the complexes; no antimicrobial activity was observed under these conditions. The plates were incubated for 24 hours at 37 °C for the following strains: *E. coli* ATCC 25922, *P. aeruginosa* ATCC 15422, *E. faecalis* ATCC 29212, *S. aureus* ATCC 25923, and *C. albicans* SC5314. Additionally, two oral bacterial strains, *S. mutans* PCM 2502 and *S. sanguinis* PCM 2335, were incubated anaerobically (85% N_2, 10% H_2, 5% CO_2) at 37 °C for 72 h. The optical density at 600 nm (OD600) was measured using a Spark® microplate reader (Tecan Trading AG, Switzerland). The value of MIC was defined as the lowest concentration that inhibited cell growth. Every assay was performed in triplicate.

Density functional theory (DFT) calculations

All calculations were carried out using the Gaussian 09 software. Geometry optimizations and frequency analyses were conducted in water using the B3LYP functional,[52,53] coupled with the 6-31G(d,p) basis set. For the Zn(II) ion, the default spin formalism was applied, and default Gaussian 09 values were used for numerical integration grids, SCF, and geometry optimization convergence criteria. No symmetry constraints were applied during the geometry optimizations. The nature of the stationary points was confirmed by computing vibrational frequencies to ensure they were true minima.

Results and discussion

To determine the protonation constants of the ligands and the stability constants of the complexes, a series of potentiometric titrations was performed. The coordination mode of Cu(II) ions, including the type and number of donor atoms involved, was investigated using various spectroscopic techniques, including UV-vis, circular dichroism, and electron paramagnetic resonance spectroscopies. The stoichiometry of the complexes formed with Zn(II) and Cu(II) ions was confirmed using electrospray ionization mass spectrometry (ESI-MS). Additionally, studies were conducted to assess the secondary structure of the ligands and the potential structural changes induced by metal ion coordination. Biological assays, performed both in the absence and presence of metal ions allowed for the evaluation of the antimicrobial activity of the studied systems against oral pathogens, with a particular focus on pH conditions characteristic of the oral cavity.

Ligands' deprotonation constants

For the studied ligands – FPNPHQPPKHPDK (L1), FPNPHQPPK (L2), and HPDK (L3) – potentiometric titrations determined 9, 4, and 5 deprotonation constants, respectively, as summarized in Table 1. The distribution diagrams of ligand species as a function of pH are presented in Fig. S3. The deprotonation constants obtained for peptides L2 and L3 are comparable to those of the corresponding amino acid residues in L1. $A_{\|}$ obtained pK_a values are consistent with literature data.[54–57]

Table 1 Deprotonation constants (pK_a) for L1, L2, and L3 peptides and stability constants ($\log\beta$) for their complexes with Cu(II) and Zn(II) ions in aqueous solution of 0.004 M $HClO_4$ with I = 0.1 M $NaClO_4$ at 25 °C. C_L = 0.0004 M. The standard deviations are reported in parentheses as uncertainties on the last significant figure. R – corresponds to amino-acid residues and C-t and N-t correspond to C-terminus and N-terminus, respectively

Ligands											
L1 (FPNPHQPPKHPDK)				L2 (FPNPHQPPK)				L3 (HPDK)			
Species	$\log\beta_{jk}$ [a]	pK_a [b]	R	Species	$\log\beta_{jk}$ [a]	pK_a [b]	R	Species	$\log\beta_{jk}$ [a]	pK_a [b]	R
$[H_7L]^{5+}$	48.15(5)	3.03	C-t	$[H_4L]^{3+}$	26.63(3)	2.77	C-t	$[H_5L]^{3+}$	30.89(2)	2.99	C-t
$[H_6L]^{4+}$	45.12(5)	4.00	Asp	$[H_3L]^{2+}$	23.85(3)	6.20	His	$[H_4L]^{2+}$	27.99(2)	3.97	Asp
$[H_5L]^{3+}$	41.12(4)	6.11	His	$[H_2L]^{+}$	17.65(2)	7.81	N-t	$[H_3L]^{+}$	24.02(1)	5.76	His
$[H_4L]^{2+}$	35.01(4)	6.63	His	[HL]	9.84(1)	9.84	Lys	$[H_2L]$	18.26(1)	7.67	N-t
$[H_3L]^{+}$	28.38(5)	7.52	N-t					$[HL]^{-}$	10.59(1)	10.59	Lys
$[H_2L]$	20.86(3)	10.15	Lys								
$[HL]^{-}$	10.71(5)	10.71	Lys								

Cu(II) complexes									
	$\log\beta_{jk}$ [c]	pK_a [d]		$\log\beta_{jk}$ [c]	pK_a [d]		$\log\beta_{jk}$ [c]	pK_a [d]
$[CuH_3L]^{3+}$	34.64(3)	—						
$[CuH_2L]^{2+}$	28.38(4)	6.26	$[CuH_2L]^{3+}$	22.04(4)	—			
$[CuHL]^{+}$	20.05(7)	8.33	$[CuHL]^{2+}$	16.92(1)	5.12	$[CuHL]^{+}$	19.95(2)	—
$[CuL]$	11.67(5)	8.38	$[CuL]^{+}$	9.07(2)	7.85	$[CuL]$	12.56(5)	7.39
$[CuH_{-1}L]^{-}$	1.51(7)	10.16	$[CuH_{-1}L]$	−0.16(2)	9.23	$[CuH_{-1}L]^{-}$	−2.56(6)	10.00
$[CuH_{-2}L]^{2-}$	−9.44(8)	10.95	$[CuH_{-2}L]^{-}$	−10.22(2)	10.06	$[CuH_{-2}L]^{2-}$	−8.29(6)	10.85

Zn(II) complexes								
	$\log\beta_{jk}$ [c]	pK_a [d]		$\log\beta_{jk}$ [c]	pK_a [d]		$\log\beta_{jk}$ [c]	pK_a [d]
$[ZnH_3L]^{3+}$	31.54(4)	—						
$[ZnH_2L]^{2+}$	24.93(1)	6.61						
						$[ZnHL]^{+}$	15.79(2)	—
$[ZnL]$	7.77(1)	—				$[ZnL]$	6.76(3)	9.03
			$[ZnH_{-1}L]$	−2.74(1)	—			
$[ZnH_{-2}L]^{2-}$	−13.25(5)	—						

[a] Constants are presented as cumulative $\log\beta_{jk}$ values. $\beta(H_jL_k) = [H_jL_k]/([H]^j[L]^k)$, in which [L] is the concentration of the fully deprotonated peptide. [b] pK_a values of the peptides were derived from cumulative constants: $pK_a = \log\beta(H_jL_k) - \log\beta(H_{j-1}L_k)$. [c] Cu(II) and Zn(II) stability constants are presented as cumulative $\log\beta_{ijk}$ values. L stands for a fully deprotonated peptide ligand that binds Cu(II)/Zn(II) ion: $\beta(M_iH_jL_k) = [M_iH_jL_k]/([M]^i[H]^j[L]^k)$, where [L] is the concentration of the fully deprotonated peptide. [d] $pK_a = \log\beta(M_iH_jL_k) - \log\beta(M_iH_{j-1}L_k)$.

Cu(II) complexes

Based on the obtained ESI-MS spectra, it can be concluded that, under the applied measurement conditions, only equimolar complexes were detected for all studied systems with Cu(II) ions (Fig. S4–S6, Table S1).

Potentiometric studies of Cu(II) complexes also confirm the absence of polynuclear complexes and bis-complexes (Table 1).

In the Cu(II)–L1 system, six distinct complex species with an equimolar metal-to-ligand stoichiometry were identified in the pH range from 3.0 to 12.0 (Table 1, Fig. 3A).

The first complex species, $[CuH_3L]^{3+}$, reaches its maximum concentration at pH 5.5. The presence of a d–d transition band in the UV-vis spectrum, with the highest molar extinction coefficient at a wavelength of 682 nm (Fig. 4A), suggests that the Cu(II) is coordinated to one or, at most, two nitrogen atoms.[58] The band at 249 nm in the CD spectra (Fig. 5A) corresponds to a charge transfer transition from N_{im} to Cu(II), while the band at 677 nm suggests the coordination of an amide nitrogen from the peptide bond, supporting a donor set of $\{1N_{im}, 1N_{am}\}$ for the $[CuH_3L]^{3+}$ complex species.[59–61] The EPR spectra at pH 5.5, with parameters: $A_{\parallel}$ = 151.7 and $g_{\parallel}$ = 2.29 (Fig. S7A, Table S2) also support the 2N coordination.[58,62,63]

In the subsequent complex species, $[CuH_2L]^{2+}$ and $[CuHL]^{+}$ (with maximum concentrations at pH 7.24 and 8.36, respectively), the coordination mode remains unchanged, with only the deprotonation of the imidazole nitrogen atom of the His residue (pK_a in the free ligand = 6.63, pK_a in the complex = 6.26 for $[CuH_2L]^{2+}$) and the N-terminal amine group (pK_a in the free ligand = 7.52, pK_a in the complex = 8.3 for $[CuHL]^{+}$, Table 1) occurring. The absence of notable spectral changes (Fig. 4A and 5A, S7A; Table S2) strongly supports the proposed donor set $\{1N_{im}, 1N_{am}\}$ in these three complex species.

In contrast, significant spectral changes occur at approximately pH 9, where the next dominant complex species, [CuL], is observed (Fig. 3A). The presence of a d–d transition band in

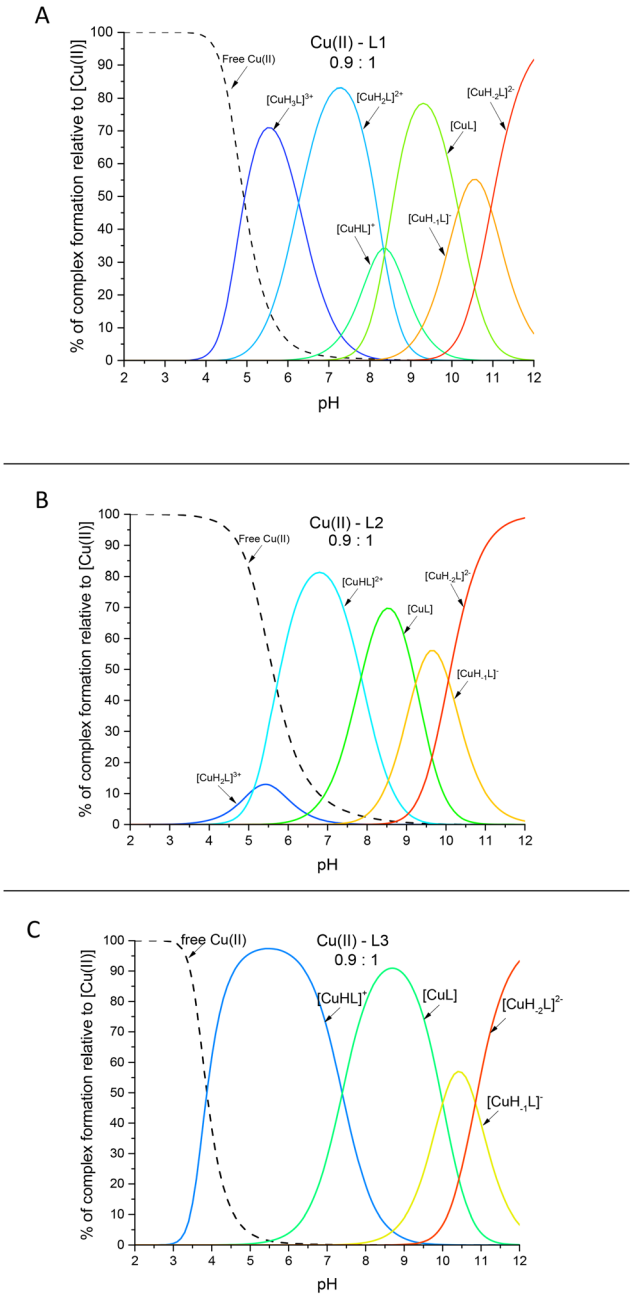

Fig. 3 Representative distribution diagram for (A) Cu(II)–L1 (FPNPHQPPKHPDK); (B) Cu(II)–L2 (FPNPHQPPK) and (C) Cu(II)–L3 (HPDK) systems in aqueous solution of 0.004 M $HClO_4$ with I = 0.1 M $NaClO_4$. [L] = 0.0004 M; molar ratio M : L – 0.9 : 1. T = 25 °C.

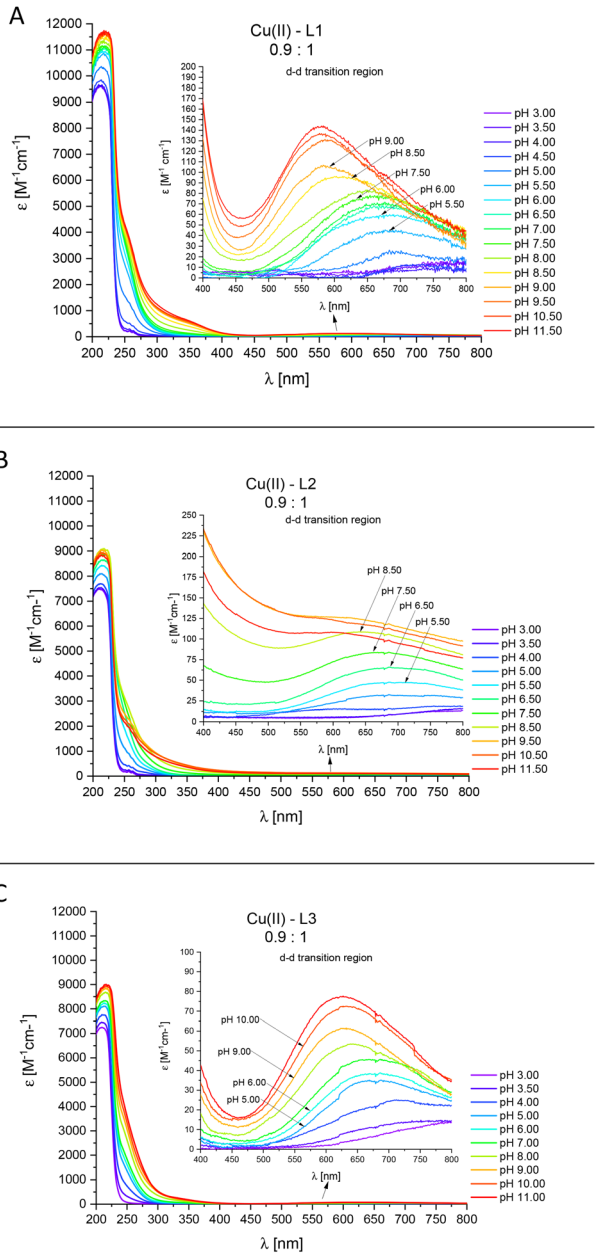

Fig. 4 UV-vis spectra for (A) Cu(II)–L1 (FPNPHQPPKHPDK), (B) Cu(II)–L2 (FPNPHQPPK), and (C) Cu(II)–L3 (HPDK) complexes. The molar ratio of M : L is 0.9 : 1, with [L] = 0.0004 M. Measurements were conducted in an aqueous $HClO_4$ solution (0.004 M) with an ionic strength of I = 0.1 M, adjusted using $NaClO_4$, at T = 25 °C. The optical path length was 1 cm. The peptides and their complexes with Cu(II) ions exhibited high solubility, and no turbidity or precipitation was observed across the entire pH range studied.

the absorption spectrum at 586 nm with ε = 105.44 M^{-1} cm^{-1} suggests Cu(II) coordination by three nitrogen donors (Fig. 4A). Additionally, the positive Cotton effect at λ = 315 nm and the negative one at 592 nm indicate the involvement of an additional nitrogen atom from the peptide bond. The EPR spectral parameters ($A_{\|}$ = 163.9 and 170.0, $g_{\|}$ = 2.27 and 2.23, Fig. S7D) suggest the coexistence of two equilibrium complex species with 2N and 3N coordination modes, which is consistent with the species distribution diagram at pH 9 (Fig. 3A). The formation of subsequent complex species, $[CuH_{-1}L]^{-}$ and $[CuH_{-2}L]^{2-}$, does not induce spectral changes, indicating that only the deprotonation of Lys residues in the peptide occurs while the coordination mode remains unchanged.

The first complex species formed in the Cu(II)–L2 system, where L2 corresponds to the N-terminal fragment of L1

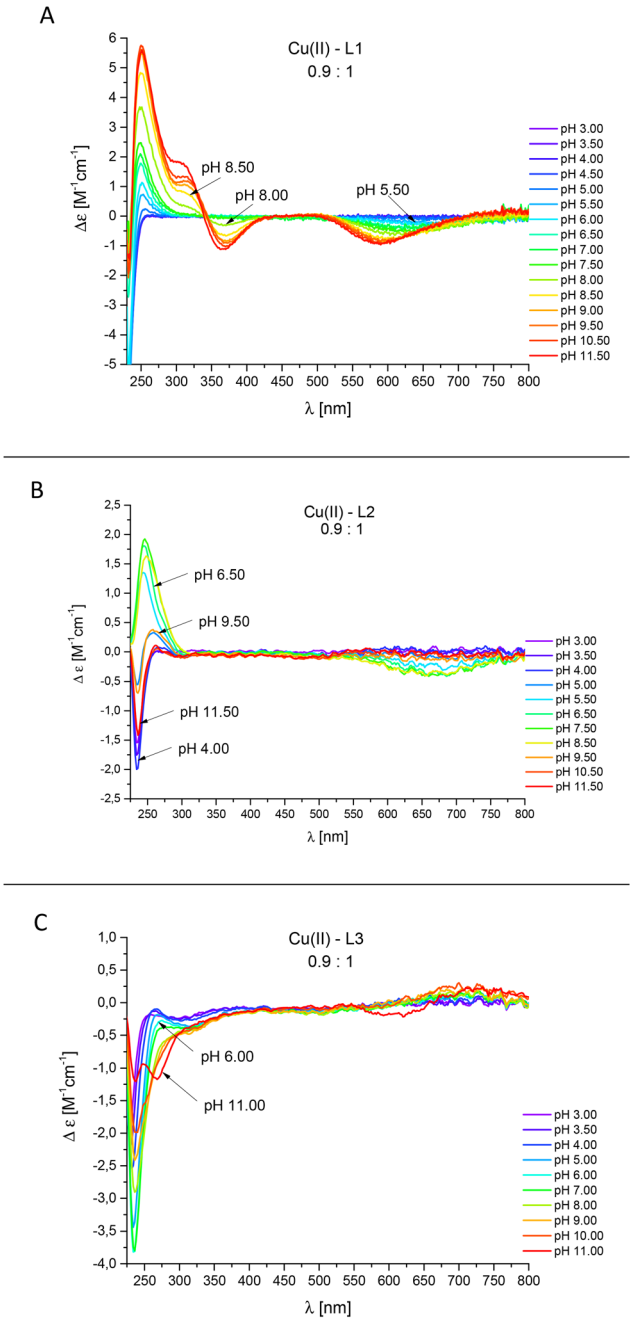

Fig. 5 CD spectra in the UV-vis range for (A) Cu(II)–L1 (FPNPHQPPKHPDK), (B) Cu(II)–L2 (FPNPHQPPK), and (C) Cu(II)–L3 (HPDK) complexes. The molar ratio of M : L is 0.9 : 1, with [L] = 0.0004 M. Measurements were conducted in an aqueous $HClO_4$ solution (0.004 M) with an ionic strength of I = 0.1 M, adjusted using $NaClO_4$, at T = 25 °C. The optical path length was 1 cm.

(FPNPHQPPK), is $[CuH_2L]^{3+}$. This species is most likely formed *via* the coordination of Cu(II) to the imidazole nitrogen ($1N_{im}$). The involvement of the imidazole nitrogen in Cu(II) coordination is supported by a strong absorption band with a maximum at 245 nm in the CD spectrum (Fig. 5B), the presence of a d–d transition band in the UV-vis spectrum with a maximum at approximately 703 nm (Fig. 4B), as well as EPR spectral parameters ($g_{\|}$ = 2.33, $A_{\|}$ = 160.7) at pH 5 (Fig. S7B).

The second complex species, $[CuHL]^{2+}$, which reaches its maximum concentration at pH 7, is most likely formed due to the deprotonation of the amide nitrogen, as indicated by the presence of an absorption band with a maximum at 676 nm (Fig. 4B) and the EPR spectral parameters ($g_{\|}$ = 2.29, $A_{\|}$ = 164.7, Fig. S7B). Circular dichroism analysis reveals bands at 245 nm and 686 nm – similar to those observed in the Cu(II)–L1 system in the pH range of 5–8 (Fig. 5) – which correspond to the involvement of imidazole and amide nitrogen atoms, respectively, forming a $\{1N_{im}, 1N_{am}\}$ donor set. The next species, $[CuL]^{+}$, which reaches its maximum concentration at pH 8.55, likely results from the deprotonation of the N-terminal amino group of the peptide. However, this group does not participate in Cu(II) coordination, as evidenced by the similar pK_a values for the N-terminus in both the free ligand and the Cu(II) complex (pK_a = 7.81 and pK_a = 7.85, respectively). Furthermore, the lack of spectral changes in the UV-vis and CD spectra, along with similar EPR parameters, confirms the suggested 2N coordination mode, with the same donor set $\{1N_{im}, 1N_{am}\}$ as in $[CuHL]^{2+}$. Another complex species, $[CuH_{-1}L]$, is most likely formed due to the deprotonation of a water molecule present in the coordination sphere of the Cu(II) ion, resulting in a donor set of $\{1N_{im}, 1N_{am}, 1OH^{-}\}$. The absence of significant spectral changes further supports this coordination mode. Finally, the formation of the last complex species, $[CuH_{-2}L]^{-}$, is attributed to the deprotonation of a lysine residue, which does not participate in Cu(II) coordination.

An intriguing phenomenon is the remarkable similarity of CD spectra at relatively extreme pH values, such as 3.5 and 10.5, as well as 5.0 and 9.5 (Fig. S8). In both cases, the spectra almost completely overlap. The complex at pH 3.5 and 10.5 exhibits bands at the same wavelengths: 266 nm and 236 nm (Fig. S8A). A similar trend is observed for the second pH pair (5.0 and 9.5), where UV-range bands appear at 258 nm and 235 nm (Fig. S8B), differing only slightly in intensity. Additionally, in alkaline conditions (above pH 8.0), a broadening of bands in the UV-vis spectra (Fig. 4B) is observed, particularly in the longer wavelength region. This effect may be attributed to the high number of proline residues in the relatively short peptide, potentially inducing conformational changes that take place in the proximity of the Cu(II) coordination sites.

The first complex species, $[CuHL]^{+}$, in the Cu(II)–L3 system (L3, HPDK – a four-amino-acid C-terminal fragment of peptide L1), is likely formed through Cu(II) coordination to the imidazole nitrogen of histidine and the N-terminal amine nitrogen, resulting in a $\{1N_{im}, -NH_2\}$ donor set. Evidence for 2N coordination includes: (i) a d–d transition band in the UV-vis spectrum with a maximum absorption at 678 nm (Fig. 4C) and (ii) EPR spectral parameters ($g_{\|}$ = 2.29, $A_{\|}$ = 163.8) at pH 6 (Fig. S6C). The involvement of the imidazole nitrogen is further supported by negative Cotton effect bands at 235 nm and ~315 nm in the CD spectrum (Fig. 5C). Additionally, the

negative Cotton effect band at 276 nm indicates the participation of the N-terminal amine group in Cu(II) coordination.[64] The formation of the subsequent species, [CuL] and $[CuH_{-1}L]^{-}$, is accompanied by the sequential deprotonation of two water molecules occupying the Cu(II) coordination sphere. The absence of additional nitrogen coordination is confirmed by spectroscopic parameters characteristic of 2N coordination (Table S2). The involvement of the imidazole nitrogen in Cu(II) binding is evidenced by CD bands at approximately 235 nm and 320 nm: at 236 nm and 319 nm for [CuL], and at 238 nm and 324 nm for $[CuH_{-1}L]^{-}$. These CD bands in the UV region likely obscure signals corresponding to the participation of the N-terminal amino group, whose maxima are expected in the 260–280 nm range.[64] The final species, $[CuH_{-2}L]^{2-}$, is formed through the deprotonation of the lysine residue, with a pK_a value of 10.85, comparable to the corresponding pK_a of the free peptide (10.59). This species retains the same coordination mode as the preceding complexes, involving the imidazole nitrogen and the N-terminal amino nitrogen, along with two deprotonated water molecule, giving $\{1N_{im}, -NH_2, 2OH^-\}$ donor set. For all species, the CD spectra exhibit a positive Cotton effect band with a maximum at approximately 700 nm (705 nm, 704 nm, 700 nm, and 708 nm for each respective species), indicative of 'histamine-like' coordination (characterized by coordination through the N-terminal amine group and the imidazole nitrogen), which further supports the proposed binding mode.[65,66]

The competition plot (Fig. 6), which compares the efficiency of Cu(II) ion binding to the ligands studied in this work, indicates that Cu(II) ions coordinated in a 'histamine-like' manner in L3 form the most stable complexes. In contrast, complexes with peptide L2 exhibit the lowest Cu(II) binding efficiency.

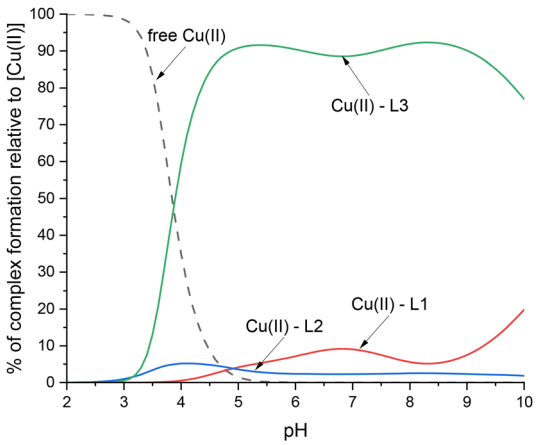

Fig. 6 Competition plot between L1 (FPNPHQPPKHPDK), L2 (FPNPHQPPK), and L3 (HPDK) with Cu(II) ions describing complex formation at different pH values in a hypothetical situation, in which equimolar amounts of all the reagents are mixed. Conditions: T = 25 °C, [Cu(II)] = [L1] = [L2] = [L3] = 0.001 M.

Zn(II) complexes

Obtained ESI-MS spectra of all systems confirmed the formation of only equimolar species of complexes under applied conditions (Fig. S9–S11, Table S1).

Calculations based on fitting the titration curves indicate the formation of four complex species in Zn(II)–L1 system within the pH range of 4 to 11 (Table 1, Fig. 7A). The first species, $[ZnH_3L]^{3+}$, appears below pH 5 and reaches its

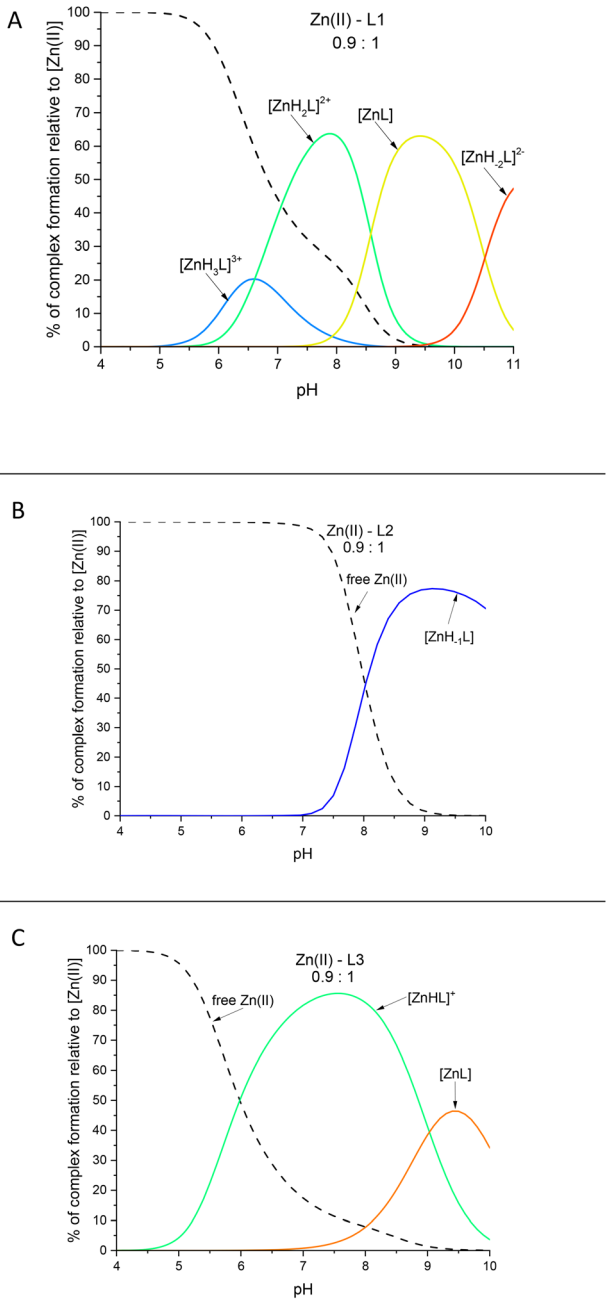

Fig. 7 Representative distribution diagram for (A) Zn(II)–L1 (FPNPHQPPKHPDK); (B) Zn(II)–L2 (FPNPHQPPK) and (C) Zn(II)–L3 (HPDK) systems in aqueous solution of 0.004 M $HClO_4$ with I = 0.1 M $NaClO_4$. [L] = 0.0004 M; molar ratio M : L – 0.9 : 1. T = 25 °C.

maximum concentration at pH 6.5. Most likely, in this complex species, the zinc ion is coordinated by two imidazole nitrogen atoms in the $\{2N_{im}\}$ or $\{1N_{im}, -NH_2\}$ donor set. The loss of a proton from the N-terminus (if it was not previously involved in coordination) or deprotonation of a water molecule leads to the formation of $[ZnH_2L]^{2+}$.

A comparison of the pK_a values of the N-terminal amino group in L1 and Zn(II)–L1 (pK_a 7.52 for the free ligand *vs.* 6.61 in the complex) may suggest involvement of this group in Zn(II) coordination. However, a similar pK_a is also observed for a deprotonation of a water molecule in the Zn(II) coordination sphere.[67] Moreover, the possibility of deprotonation of a non-coordinating histidine residue (if it was not previously involved in coordination) – whose side chain exhibits a pK_a of 6.63 in the free ligand – cannot be excluded, making unambiguous assignment of the deprotonation event challenging.

At pH values above 9, the [ZnL] species dominates in solution. This species likely arises from deprotonation of a coordinated water molecule and the N-terminal amino group – provided the latter was not already involved in coordination – or alternatively, from deprotonation of an additional water molecule. These equilibria may result in a complex with one of several donor sets: $\{2N_{im}, -NH_2, 1OH^-\}$, $\{1N_{im}, -NH_2, 2OH^-\}$, or $\{2N_{im}, 2OH^-\}$, with the latter two coordination modes appearing more plausible considering that Zn(II) typically prefers a coordination number of four over five.[68] The last detected species, ($[ZnH_{-2}L]^{2-}$), forms as a result of deprotonation of the nonbonding two lysine side chains.

Density functional theory (DFT) calculations were employed to resolve the aforementioned question regarding the coordination mode of Zn(II) ions by ligand L1. The results of the calculations indicate that the first species, $[ZnH_3L]^{3+}$ (pH range 5–6.5), may be assigned to the zinc ion coordinated by two imidazole nitrogen atoms in the $\{2N_{im}\}$ donor set. At this, and higher pH values, involvement of N-terminus binding to the Zn(II) ion (resulting in a $\{1N_{im}, -NH_2\}$ donor set) could be excluded due to the rigidity of the peptide associated with the presence of several prolines. Indeed, structures involving a $\{1N_{im}, -NH_2\}$ donor set could never converge in the calculations, indicating that this binding mode is of relatively high energy on the potential energy surface.

In a pH range 7–8, the $[ZnH_2L]^{2+}$ species is best described as having the Zn(II) ion coordinated to the $\{2N_{im}\}$ donor set, in a mixed species characterized by either loss of a proton from the N-terminus or with a deprotonated water molecule in the ion coordination sphere. In this latter case, deprotonation occurs for H_A (Fig. 8), the only H atom not involved in H-bonding with the peptide. The two species differing by only 6.7 kcal mol^{-1} (28 kJ mol^{-1}), with the former (N-terminus deprotonation) being more stable, are likely in equilibrium. The small calculated energy difference supports the experimentally measured similar pK_a values for the two deprotonation steps.

At pH values above 9, following the previous two deprotonations, the lowest energy [ZnL] species features a $\{2N_{im}, 2OH^-\}$ donor set with a deprotonated N-terminal amino group.

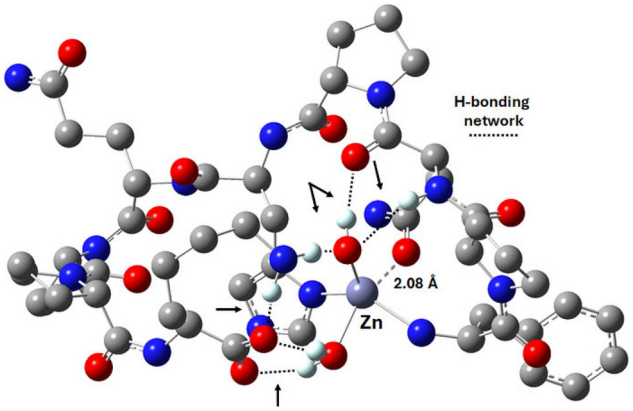

Fig. 8 DFT calculated structure of Zn(II)–L1 (FPNPHQPPKHPDK) in a water molecule at pH range 7–8.

In the Zn(II)–L2 system, only one complex species was detected [$ZnH_{-1}L$] (Table 1, Fig. 7B), which reaches its maximum concentration at pH 9.15. In this complex, the Zn(II) ion is most likely coordinated by two nitrogen atoms: one from the imidazole ring of the histidine residue and the other from the N-terminal amino group, forming an $\{1N_{im}, -NH_2\}$ donor set. Above pH 10, the formation of zinc(II) hydroxides was observed (not shown in the diagram). DFT calculations support the presence of an $\{1N_{im}, -NH_2\}$ donor set, and further reveal that the Zn(II) ion is coordinated to the L2 system in a distorted pentacoordinate geometry stabilized by an extended H-bonding network (Fig. 9). Interestingly, this binding mode appears relatively stable if a $\{OH_2, OH^-\}$ donor set completes the Zn(II) ion coordination sphere, but further deprotonation of a bound water molecule (resulting in a

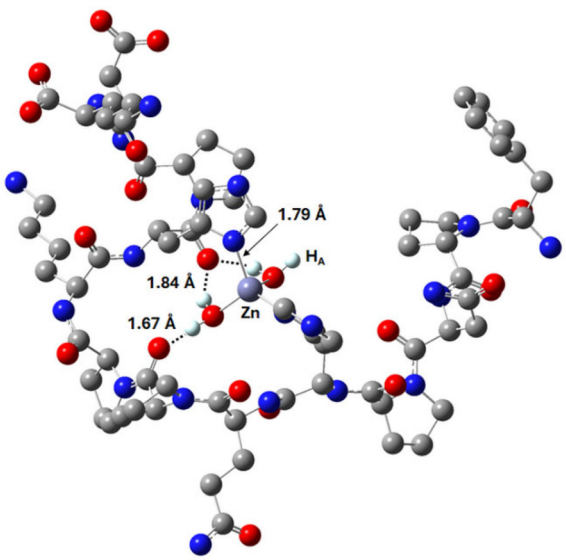

Fig. 9 DFT calculated structure of Zn(II)–L2 (FPNPHQPPK) in water at pH range 7.5–8.5.

{2OH$^-$} donor set) distorts the complex to a geometry unlike to be persistent in solution, and therefore leading to the formation of zinc(II) hydroxides, as experimentally observed.

In the Zn(II)–L3 system, the formation of two complex species was detected under the given experimental conditions: [ZnHL]$^+$ and [ZnL] (Table 1, Fig. 7C). The first species reaches its maximum concentration at pH 7.6 and is most likely formed through the coordination of the Zn(II) by a 'histamine-like' motif, {1N$_{im}$, –NH$_2$}, similar to what has been observed with Cu(II) ions. Deprotonation of a water molecule (pK_a = 9.03) leads to the formation of the second species, [ZnL]. Above pH 9.5, the formation of zinc(II) hydroxides was observed, as in the case of the Zn(II)–L2 system (not shown in the diagram). DFT calculations strongly support these assignments (Fig. 10).

The comparison of Zn(II) binding affinity among the studied ligands (Fig. 11) demonstrates that the 'histamine-like' coordination mode observed in the Zn(II)–L3 system leads to the formation of the most stable complexes at pH values below 9. Above this pH, L1 exhibits the highest Zn(II) binding efficiency.

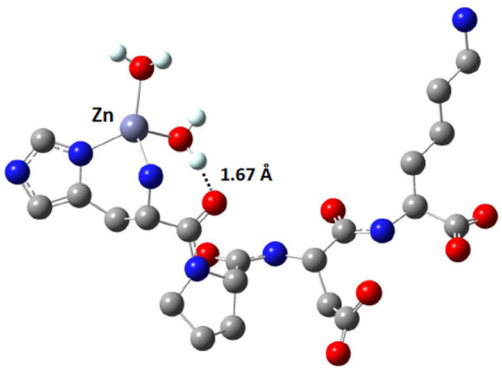

Fig. 10 DFT calculated structure of Zn(II)–L3 (HPDK) in water at pH range 6–8.5.

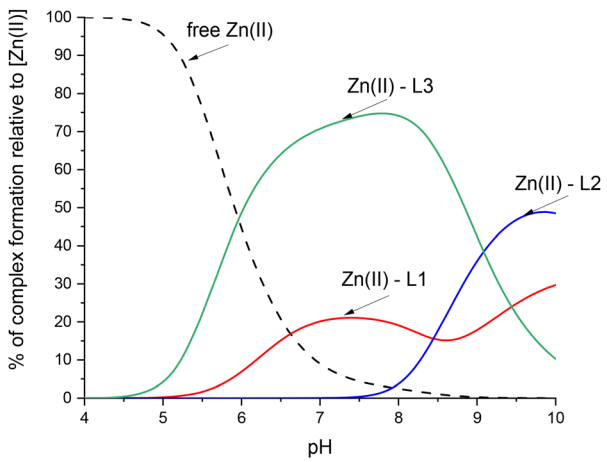

Fig. 11 Competition plot between L1 (FPNPHQPPKHPDK), L2 (FPNPHQPPK), and L3 (HPDK) with Zn(II) ions describing complex formation at different pH values in a hypothetical situation in which equimolar amounts of all the reagents are mixed. Conditions: T = 25 °C, [Zn(II)] = [L1] = [L2] = [L3] = 0.001 M.

Secondary structure

Antimicrobial peptides are often characterized by well-defined secondary structures, such as α-helices or β-sheets, which are frequently associated with enhanced antimicrobial activity.[69] Metal ions are known to induce the formation of such ordered structures upon coordination with this type of peptides.[70]

To elucidate the mechanism of antimicrobial action of a given system, characterization of its secondary structure is of critical importance. Fig. S12 presents selected far-UV CD spectra recorded for the investigated systems. None of the spectra exhibits distinct features indicative of well-ordered secondary structure formation. Only minor spectral changes were observed for the Cu(II) and Zn(II) complexes at pH ~7.4 for the L1 and L2 peptides, which may suggest a slight tendency toward the formation of polyproline type II (PPII) helices.[71] In the case of L3-based metal complexes, spectral variations were observed for the Cu(II) complexes at both pH 5.4 and 7.4 (Fig. S12C). However, the short length of the peptide sequences precludes the formation of stable and well-defined secondary structures.[72,73]

Biological activity tests

To evaluate the antimicrobial efficacy of the peptide L1 (FPNPHQPPKHPDK), its proteolytically derived fragments L2 (FPNPHQPPK) and L3 (HPDK), and their coordination complexes with Cu(II) and Zn(II) ions, a standard broth microdilution method was employed. This assay enabled the determination of the MIC, defined as the lowest concentration of a compound that visibly inhibits microbial growth. Given that human salivary pH can range from 5.3 to 7.8,[74] depending on physiological and pathological conditions, antimicrobial activity was examined at mildly acidic (pH 5.4) (Table 2, Tables S3–S10) and near-physiological (7.4) (Table 3), both of which are relevant to the oral environment.

The peptides and their metal complexes exhibited modest antibacterial activity primarily against Gram-positive bacteria, including *S. aureus*, *E. faecalis*, *S. mutans*, and *S. sanguinis*, whereas Gram-negative strains such as *E. coli* and *P. aeruginosa* remained largely resistant under both tested pH conditions (5.4 and 7.4). No antifungal activity against *C. albicans* was detected for any of the tested compounds. Free Cu(II) and Zn(II) ions at concentrations ranging from 0.5 to 65 μg mL^{-1}, corresponding to those present in the peptide–metal complexes, did not exhibit measurable antimicrobial effects against the tested bacterial strains or *C. albicans* (data not shown).

The antibacterial efficacy of the peptides was enhanced under slightly acidic conditions (pH 5.4) and upon coordi-

Table 2 The antibacterial and anti-*Candida* activities of peptides/complexes were assessed *in vitro* by determining their MIC (μg mL^{-1}). Antimicrobial tests were conducted in a 0.01 M MES buffer at pH 5.4. Experiments were performed for peptides and their copper(II) and zinc(II) complexes. N/D – not determined within the concentration range used in this study

	FPNPHQPPKHPDK (L1)			FPNPHQPPK (L2)			HPDK (L3)		
Strain	L1	+Cu(II)	+Zn(II)	L2	+Cu(II)	+Zn(II)	L3	+Cu(II)	+Zn(II)
E. coli ATCC 25922	N/D	N/D	**500**	N/D	N/D	N/D	N/D	N/D	N/D
P. aeruginosa ATCC 15422	N/D	N/D	N/D	N/D	N/D	N/D	N/D	N/D	N/D
S. aureus ATCC 25923	N/D	**500**	**500**	N/D	N/D	N/D	**500**	**500**	**500**
E. faecalis ATCC 29212	N/D	N/D	**500**	N/D	N/D	N/D	N/D	N/D	**500**
S. mutans PCM 2502	N/D	N/D	**500**	N/D	N/D	N/D	N/D	**500**	**500**
S. sanguinis PCM 2335	N/D	N/D	**500**	**500**	**250**	**250**	**500**	**125**	**125**
C. albicans SC5314	N/D	N/D	N/D	N/D	N/D	N/D	N/D	N/D	N/D

Table 3 The antibacterial and anti-*Candida* activities of peptides/complexes were assessed *in vitro* by determining their MIC (μg mL^{-1}). Antimicrobial tests were conducted in a 0.01 M HEPES buffer at pH 7.4. Experiments were performed for peptides and their copper(II) and zinc(II) complexes. N/D – not determined within the concentration range used in this study

	FPNPHQPPKHPDK (L1)			FPNPHQPPK (L2)			HPDK (L3)		
Strain	L1	+Cu(II)	+Zn(II)	L2	+Cu(II)	+Zn(II)	L3	+Cu(II)	+Zn(II)
E. coli ATCC 25922	N/D	N/D	N/D	N/D	N/D	N/D	N/D	N/D	N/D
P. aeruginosa ATCC 15422	N/D	N/D	N/D	N/D	N/D	N/D	N/D	N/D	N/D
E. faecalis ATCC 29212	N/D	N/D	N/D	N/D	N/D	N/D	N/D	N/D	N/D
S. aureus ATCC 25923	N/D	N/D	N/D	N/D	N/D	N/D	N/D	N/D	N/D
S. mutans PCM 2502	N/D	N/D	N/D	N/D	N/D	N/D	N/D	N/D	N/D
S. sanguinis PCM 2335	N/D	N/D	**500**	N/D	N/D	**500**	N/D	N/D	**250**
C. albicans SC5314	N/D	N/D	N/D	N/D	N/D	N/D	N/D	N/D	N/D

nation with metal ions, particularly for peptide L1 and its C-terminal fragment L3 (HPDK). The most notable effects were observed against *S. aureus*, *S. sanguinis*, and *S. mutans*. The increased activity of L3 may be attributed to its higher metal-binding capacity, possibly facilitated by a histamine-like binding motif. This interaction is consistent with the mechanism of nutritional immunity, wherein sequestration of essential metal ions by host peptides or proteins limits microbial access to these nutrients, thereby inhibiting microbial growth and virulence.[75] Nutritional immunity is a critical innate defense strategy in which the host tightly regulates and restricts the availability of transition metals such as zinc and copper, which are essential cofactors for numerous microbial enzymes and metabolic processes. By forming stable complexes with these metal ions, peptides like L3 may mimic this natural defense mechanism, effectively starving pathogens of necessary nutrients and reducing their ability to proliferate. This mode of action complements direct antimicrobial effects and highlights the multifunctional nature of metal-binding peptides in host defense.

This observation is consistent with previous studies demonstrating that metal ion binding can enhance bactericidal activity.[69,76] A similar effect has been reported in the design of synthetic antimicrobial peptides, where coordination to transition metals such as Zn(II) and Cu(II) improves both peptide stability and antimicrobial efficacy.[38–41]

Among the compounds tested, peptide L1 showed moderate antimicrobial activity in combination with Zn(II) at pH 5.4, with MIC values around 500 μg mL^{-1}. Peptide L2 exhibited limited activity, restricted to *S. sanguinis*, but its metal complexes displayed improved potency with MIC values reduced to approximately 250 μg mL^{-1}. Peptide L3 and its metal complexes demonstrated the highest antibacterial activity under mildly acidic conditions, particularly against *S. sanguinis*, with MIC values as low as 125 μg mL^{-1}. These findings suggest that the full-length peptide sequence may not be essential for antimicrobial activity and highlight the critical role of metal coordination in enhancing this function. At near-physiological pH (7.4), only the Zn(II) complexes of L1, L2, and L3 showed detectable activity against *S. sanguinis*. This bacterium is a well-known oral pathogen implicated in dental plaque formation and associated oral diseases such as caries and periodontitis.[77,78]

Therefore, the selective activity against *S. sanguinis* under both acidic and physiological pH conditions could be relevant for oral therapeutic strategies that aim to target cariogenic bacteria without broadly disrupting the oral microbiome. While no antifungal effects were observed, the specificity of these peptides and their complexes toward Gram-positive bacteria may be advantageous for the development of narrow-spectrum antimicrobials. The lack of antimicrobial activity from free Cu(II) and Zn(II) ions confirms that the enhanced effects arise

from peptide–metal complexation rather than from metal ion toxicity alone.

Conclusions

Coordination of Zn(II) and Cu(II) ions to the antimicrobial peptide, FPNPHQPPKHPDK, and the two products of its hydrolysis leads to distinct structural and biological outcomes. DFT calculations provided insights into the structures of the observed coordination preferences and pH-dependent speciation, supporting the formation of specific donor sets in each Zn(II)–peptide system: $\{2N_{im}\}$ for L1, $\{1N_{im}, -NH_2\}$ for L2, and a histamine-like $\{1N_{im}, -NH_2\}$ motif for L3 at near-physiological pH.

The antimicrobial activity of the tested peptides was enhanced in the presence of metal ions and exhibited selectivity toward Gram-positive bacteria, with increased efficacy observed under slightly acidic conditions (pH 5.4), which reflect the oral environment. Notably, Zn(II) coordination significantly improved the antimicrobial properties of peptide L1, particularly against *S. aureus*, *E. faecalis*, and *S. sanguinis*, as confirmed by MIC values. In contrast, Cu(II) did not produce a comparable effect under the same conditions, suggesting a specific role of Zn(II) in modulating the antimicrobial potential of L1.

Although CD spectra indicated no substantial changes in the global secondary structure upon metal coordination, the differences in biological activity suggest that more localized factors may be involved. These could include subtle conformational rearrangements, altered charge distribution, or modifications in peptide–membrane interactions. Such mechanisms are currently under further investigation.

Among the studied peptides, HPDK (L3) demonstrated the highest antimicrobial potency and thermodynamic stability when complexed with either Cu(II) or Zn(II) (histamine-like binding mode). The minor conformational changes observed in the CD spectra of the Cu(II)–L3 system are unlikely to fully account for the antimicrobial activity, which is more plausibly attributed to a 'nutritional immunity' mechanism, whereby strong and stable metal–ligand complexation reduces the availability of essential metal ions to microbes, thus impairing their growth. In contrast, the other peptides appear to coordinate metal ions through a less specific binding mode, likely resulting in lower complex stability and consequently a reduced or different pattern of antimicrobial activity.

Peptides obtained through proteolytic processing retained the bioactivity of the parent sequence. In some cases, improved MIC values and enhanced complex stability were observed, indicating that naturally derived peptide fragmentation can yield products with optimized functional properties. This reinforces the concept of biological efficiency in the design of host defense peptides.

The lack of antimicrobial activity against Gram-negative bacteria and *C. albicans* highlights the specificity of these systems toward selected bacterial targets. For the less active systems, we do not exclude the possibility that their function may involve interactions with intracellular targets or modulation of neighboring sequence regions within the native MUC7 protein. These aspects will be addressed in future stages of the research. Furthermore, targeted structural modifications of peptide L1 or refinement of its metal-binding properties may provide a means to enhance and broaden its antimicrobial spectrum.

Author contributions

The manuscript was written through the contributions of all authors. All authors have given approval to the final version of the manuscript.

Conflicts of interest

The authors declare no competing financial interest.

Data availability

The data supporting this study, including trypsin digestion tests, certificates of analysis of synthesized peptides, potentiometric titrations, mass spectrometry results, EPR spectra, far-UV CD spectra, are available in the SI. Biological assay data related to antimicrobial activity are provided within the main article and SI. No restrictions apply to the availability of these data. If any additional questions regarding experimental details may arise, the corresponding author remains at the Readers' disposal.

MALDI mass spectra of the FPN peptide after trypsin digestion; certificates of analysis of synthesized peptides; thermodynamic and spectroscopic data for proton of MUC7 fragments, potentiometric titration curves for MUC7 fragments, mass spectra for the metal–peptide systems; EPR spectra for Cu(II)-MUC7 fragments and its Cu(II) complexes, CD spectra in the far-UV (180–250 nm) region at chosen pH values and biological growth inhibition tests performed with the studied peptides and their metal complexes at various concentrations (μg mL^{-1}) at pH 5.4 and 7.4. See DOI: **https://doi.org/10.1039/d5dt01418b**.

Acknowledgements

The authors thank the National Science Centre (grant no. UMO-2021/41/B/ST4/02654, J. W.) for financial support. We would also like to thank prof. Elżbieta Gumienna-Kontecka from the University of Wrocław for kindly providing access to the Jasco J-1500 CD spectropolarimeter.

References

1 I. Dozic and T. Todorovic, *Stomatol. Glas. Srb.*, 2005, **52**, 208–216.
2 S. Baliga, S. Muglikar and R. Kale, *J. Indian Soc. Periodontol.*, 2013, **17**, 461.
3 I. M. Dawood and S. K. El-Samarrai, *Int. J. Adv. Res. Biol. Sci.*, 2018, **5**, 1–45.
4 C. Dawes and D. T. W. Wong, *J. Dent. Res.*, 2019, **98**, 133–141.
5 P. Pandey, N. Reddy, V. Rao, A. Saxena and C. Chaudhary, *Contemp. Clin. Dent.*, 2015, **6**, 65.
6 S. C. Durso, L. M. Vieira, J. N. S. Cruz, C. S. Azevedo, P. H. Rodrigues and M. R. L. Simionato, *Caries Res.*, 2014, **48**, 214–222.
7 L. Babaeekhou, A. A. Mehrizi and M. Ghane, *Dent. Res. J.*, 2020, **17**, 134–141.
8 N. Izadi, M. Keikha, K. Ghazvini and M. Karbalaei, *Gene Rep.*, 2020, **21**, 100811.
9 Z. Khurshid, M. Naseem, Z. Sheikh, S. Najeeb, S. Shahab and M. S. Zafar, *Saudi Pharm. J.*, 2016, **24**, 515–524.
10 M. Mori, H. Takeuchi, M. Sato and S. Sumitomo, *Oral Med. Pathol.*, 2006, **11**, 1–17.
11 R. B. Brown and M. A. Hollingsworth, in *Encyclopedia of Biological Chemistry*, Elsevier, 2013, pp. 200–204.
12 Y. Liu, X. Yu, J. Zhao, H. Zhang, Q. Zhai and W. Chen, *Int. J. Biol. Macromol.*, 2020, **164**, 884–891.
13 N. Jonckheere, N. Skrypek, F. Frénois and I. Van Seuningen, *Biochimie*, 2013, **95**, 1077–1086.
14 J. A. Voynow and B. M. Fischer, in *Encyclopedia of Respiratory Medicine*, Elsevier, 2006, pp. 56–62.
15 E. P. Bennett, U. Mandel, H. Clausen, T. A. Gerken, T. A. Fritz and L. A. Tabak, *Glycobiology*, 2012, **22**, 736–756.
16 E. S. Frenkel and K. Ribbeck, *J. Oral Microbiol.*, 2015, **7**, 29759.
17 R. R. Hodges and D. A. Dartt, *Exp. Eye Res.*, 2013, **117**, 62–78.
18 T. L. Gururaja, N. Ramasubbu, P. Venugopalan, M. S. Reddy, K. Ramalingam and M. J. Levine, *Glycoconjugate J.*, 1998, **15**, 457–467.
19 B. Liu, S. A. Rayment, C. Gyurko, F. G. Oppenheim, G. D. Offner and R. F. Troxler, *Biochem. J.*, 2000, **345**(Pt 3), 557–564.
20 A. Janicka-Kłos, T. Janek, J. Burger and H. Czapor-Irzabek, *J. Inorg. Biochem.*, 2020, **203**, 110923.
21 L. Bobek and H. Situ, *Antimicrob. Agents Chemother.*, 2003, **47**, 643–652.
22 J. Satyanarayana, H. Situ, S. Narasimhamurthy, N. Bhayani, L. A. Bobek and M. J. Levine, *J. Pept. Res.*, 2000, **56**, 275–282.
23 S. Takehara, M. Yanagishita, K. A. Podyma-Inoue and Y. Kawaguchi, *PLoS One*, 2013, **8**, e69059.
24 P. Wang, L. Hu, G. Liu, N. Jiang, X. Chen, J. Xu, W. Zheng, L. Li, M. Tan, Z. Chen, H. Song, Y.-D. Cai and K.-C. Chou, *PLoS One*, 2011, **6**, e18476.
25 Q.-Y. Zhang, Z.-B. Yan, Y.-M. Meng, X.-Y. Hong, G. Shao, J.-J. Ma, X.-R. Cheng, J. Liu, J. Kang and C.-Y. Fu, *Mil. Med. Res.*, 2021, **8**, 48.
26 M. Mardirossian, N. Pérébaskine, M. Benincasa, S. Gambato, S. Hofmann, P. Huter, C. Müller, K. Hilpert, C. A. Innis, A. Tossi and D. N. Wilson, *Cell Chem. Biol.*, 2018, **25**, 530–539.
27 M. G. Gagnon, R. N. Roy, I. B. Lomakin, T. Florin, A. S. Mankin and T. A. Steitz, *Nucleic Acids Res.*, 2016, **44**, 2439–2450.
28 T. Florin, C. Maracci, M. Graf, P. Karki, D. Klepacki, O. Berninghausen, R. Beckmann, N. Vázquez-Laslop, D. N. Wilson, M. V. Rodnina and A. S. Mankin, *Nat. Struct. Mol. Biol.*, 2017, **24**, 752–757.
29 A. Bennick, *Mol. Cell. Biochem.*, 1982, **45**, 83–99.
30 A. M. Lynge Pedersen and D. Belstrøm, *J. Dent.*, 2019, **80**, 3–12.
31 L. D. Pettit, I. Steel, G. Formicka-Kozlowska, T. Tatarowski and M. Bataille, *J. Chem. Soc., Dalton Trans.*, 1985, 535–539.
32 R. Bhattacharyya and P. Chakrabarti, *J. Mol. Biol.*, 2003, **331**, 925–940.
33 C. M. Deber, B. Brodsky and A. Rath, in *Encyclopedia of Life Sciences*, Wiley, 2010.
34 W. Li, J. Tailhades, N. M. O'Brien-Simpson, F. Separovic, L. Otvos, M. A. Hossain and J. D. Wade, *Amino Acids*, 2014, **46**, 2287–2294.
35 Y. Zhu, J. C. Weisshaar and M. Mustafi, *J. Biol. Chem.*, 2020, **295**, 13314–13325.
36 A. Bin Hafeez, X. Jiang, P. J. Bergen and Y. Zhu, *Int. J. Mol. Sci.*, 2021, **22**, 11691.
37 J. Wątły, K. Szarszoń, M. Sabieraj, A. Kola, R. Wieczorek, T. Janek and D. Valensin, *Inorg. Chem.*, 2025, **64**, 6365–6377.
38 J. Wątły, K. Szarszoń, A. Mikołajczyk, M. Grelich-Mucha, A. Matera-Witkiewicz, J. Olesiak-Bańska and M. Rowińska-Żyrek, *Inorg. Chem.*, 2023, **62**, 19786–19794.
39 A. Miller, A. Matera-Witkiewicz, A. Mikołajczyk, R. Wieczorek and M. Rowińska-Żyrek, *Inorg. Chem.*, 2021, **60**, 12730–12734.
40 A. Miller, A. Matera-Witkiewicz, A. Mikołajczyk-Tarnawa, A. Kola, M. Wiloch, M. Jonsson-Niedziolka, R. Wieczorek, J. Wątły, D. Valensin and M. Rowińska-Żyrek, *Chem. Sci.*, 2025, **16**, 3447–3458.
41 D. Dudek, E. Dzień, J. Wątły, A. Matera-Witkiewicz, A. Mikołajczyk, A. Hajda, J. Olesiak-Bańska and M. Rowińska-Żyrek, *Sci. Rep.*, 2022, **12**, 20543.
42 E. J. Helmerhorst, R. F. Troxler and F. G. Oppenheim, *Proc. Natl. Acad. Sci. U. S. A.*, 2001, **98**, 14637–14642.
43 S. R. Hennigar and J. P. McClung, *Am. J. Lifestyle Med.*, 2016, **10**, 170–173.
44 H. L. Norris, J. Friedman, Z. Chen, S. Puri, G. Wilding and M. Edgerton, *J. Oral Microbiol.*, 2018, **10**, 1447216.
45 G. Gran, H. Dahlenborg, S. Laurell and M. Rottenberg, *Acta Chem. Scand.*, 1950, **4**, 559–577.
46 P. Gans, A. Sabatini and A. Vacca, *Talanta*, 1996, **43**, 1739–1753.
47 C. Baes and R. Mesmer, *The Hydrolysis of Cations*, Wiley, New York, 1976.

48 L. Alderighi, P. Gans, A. Ienco, D. Peters, A. Sabatini and A. Vacca, *Coord. Chem. Rev.*, 1999, **184**, 311–318.
49 OriginLab Corporation, *Origin(Pro), Version 2024*, Northampton, MA, USA, 2024.
50 A. M. Gillum, E. Y. H. Tsay and D. R. Kirsch, *Mol. Gen. Genet.*, 1984, **198**, 179–182.
51 I. Wiegand, K. Hilpert and R. E. W. Hancock, *Nat. Protoc.*, 2008, **3**, 163–175.
52 P. J. Stephens, F. J. Devlin, C. F. Chabalowski and M. J. Frisch, *J. Phys. Chem.*, 1994, **98**, 11623–11627.
53 A. D. Becke, *J. Chem. Phys.*, 1993, **98**, 5648–5652.
54 B. Orzel, M. Ostrowska, S. Potocki, M. A. Zoroddu, H. Kozlowski, M. Peana and E. Gumienna-Kontecka, *Inorg. Chem.*, 2025, **64**, 5038–5052.
55 H. Kozłowski, T. Kowalik-Jankowska and M. Jeżowska-Bojczuk, *Coord. Chem. Rev.*, 2005, **249**, 2323–2334.
56 J. Watly, E. Simonovsky, N. Barbosa, M. Spodzieja, R. Wieczorek, S. Rodziewicz-Motowidlo, Y. Miller and H. Kozlowski, *Inorg. Chem.*, 2015, **54**, 7692–7702.
57 M. Peana, E. Gumienna-Kontecka, F. Piras, M. Ostrowska, K. Piasta, K. Krzywoszynska, S. Medici and M. A. Zoroddu, *Inorg. Chem.*, 2020, **59**, 4661–4684.
58 L. D. Pettit, J. E. Gregor and H. Kozlowski, *ChemInform*, 1992, **1**, 1–41.
59 K. Zavitsanos, A. M. P. C. Nunes, G. Malandrinos, C. Kállay, I. Sóvágó, V. Magafa, P. Cordopatis and N. Hadjiliadis, *Dalton Trans.*, 2008, 6179.
60 B. Belosi, E. Gaggelli, R. Guerrini, H. Kozłowski, M. Łuczkowski, F. M. Mancini, M. Remelli, D. Valensin and G. Valensin, *ChemBioChem*, 2004, **5**, 349–359.
61 K. Szarszoń, S. Andrä, T. Janek and J. Wątły, *Inorg. Chem.*, 2024, **63**, 11616–11627.
62 J. Peisach and W. E. Blumberg, *Arch. Biochem. Biophys.*, 1974, **165**, 691–708.
63 H. Sigel and R. B. Martin, *Chem. Rev.*, 1982, **82**, 385–426.
64 J.-F. Galey, H. Kozlowski and L. D. Pettit, *J. Inorg. Biochem.*, 1991, **44**, 149–153.
65 I. Török, T. Gajda, B. Gyurcsik, G. K. Tóth and A. Péter, *J. Chem. Soc., Dalton Trans.*, 1998, 1205–1212.
66 P. Kołkowska, A. Hecel, D. Kędzierska, M. Ostrowska, P. K. Walencik, J. Wątły, K. Zdyb, M. Spodzieja, S. Rodziewicz-Motowidło, S. Potocki, M. Łuczkowski, E. Gumienna-Kontecka and M. Rowińska-Żyrek, *J. Inorg. Biochem.*, 2016, **163**, 258–265.
67 E. Kimura, T. Gotoh, S. Aoki and M. Shiro, *Inorg. Chem.*, 2002, **41**, 3239–3248.
68 T. Dudev and C. Lim, *J. Am. Chem. Soc.*, 2000, **122**, 11146–11153.
69 L. Falcigno, S. Braccia, R. Bellavita, G. D'Auria, A. Falanga and S. Galdiero, *Front. Drug Discovery*, 2024, **4**, 1440378.
70 D. Łoboda, H. Kozłowski and M. Rowińska-Żyrek, *New J. Chem.*, 2018, **42**, 7560–7568.
71 A. Micsonai, É. Bulyáki and J. Kardos, *Methods Mol. Biol.*, 2021, **2199**, 175–189.
72 M. Seo, S. Rauscher, R. Pomès and D. P. Tieleman, *J. Chem. Theory Comput.*, 2012, **8**, 1774–1785.
73 H. I. Merritt, N. Sawyer and P. S. Arora, *Pept. Sci.*, 2020, **112**, 1–20.
74 S. Gittings, N. Turnbull, B. Henry, C. J. Roberts and P. Gershkovich, *Eur. J. Pharm. Biopharm.*, 2015, **91**, 16–24.
75 C. C. Murdoch and E. P. Skaar, *Nat. Rev. Microbiol.*, 2022, **20**, 657–670.
76 M. Adriana, M. Aleksandra, B. Denise, G. Kinga, W. Joanna, H. Aleksandra, W. Robert, M.-W. Agnieszka and R.-Ż. Magdalena, *Inorg. Chem.*, 2024, **63**, 12958–12968.
77 H. T. Pramesti, *Padjadjaran J. Dent.*, 2016, **28**, 45–52.
78 B. Zhu, L. C. Macleod, T. Kitten and P. Xu, *Future Microbiol.*, 2018, **13**, 915–932.